Proceedings of the OAGM Workshop 2018 DOI: 10.3217/978-3-85125-603-1-15

A Study of Spectral Expansion for Shape Correspondence

Robert Dachsel, Michael Breuß and Laurent Hoeltgen

Abstract— **The main task in three dimensional non-rigid shape correspondence is to retrieve similarities between two or more similar three dimensional objects. A useful way to tackle this problem is to construct a simplified shape representation, called feature descriptor, which is invariant under deformable transformations. A successful class of such feature descriptors is based on physical phenomena, concretely by the heat equation for the heat kernel signature and the Schrödinger equation for the wave kernel signature. Both approaches employ the spectral decomposition of the Laplace-Beltrami operator, meaning that solutions of the corresponding equations are expressed by a series expansion in terms of eigenfunctions. The feature descriptor is then computed at hand of those solutions. In this paper we explore the influence of the amount of used eigenfunctions on shape correspondence applications, as this is a crucial point with respect to accuracy and overall computational efficiency of the method. Our experimental study will be performed at hand of a standard shape data set.**

I. INTRODUCTION

In many tasks, it is useful to describe a three dimensional geometric object by its bounding surface, often referred as shape. Thereby, the investigation of shape correspondence is a fundamental operation in visual computing, with many potential fields of applications including medical imaging, geometric modeling and digital heritage [8], [10], [12]. For a general shape correspondence scenario there are two or more shapes given, and it is the task to find a reasonable relation/pairing between them. In the context of rigid shape correspondence, shapes may be considered similar if there exists a rigid transformation between them. Since those transformations can be represented compactly as a rotation, translation and reflection, many solution techniques are well established such as Iterative Closest Point methods, cf. [3], [6] among others. A more challenging yet oftentimes more realistic setting is that of non-rigid shape correspondence, where the shapes are able to undergo almost isometric transformations, leading to a large variety of possible deformations such as poses of human or animal bodies.

An important solution strategy to obtain pointwise shape correspondence is to employ a feature descriptor computed over each shape, and to attempt to match the values of the feature descriptor. The task of the feature descriptor is to characterize each element on the shape regarding its geometric properties. Ideally, this feature descriptor is invariant under deformable transformations, which is challenging to achieve in its construction.

Related Work. In this paper we consider a modern class of feature descriptors that can handle almost isometric transformations, namely the so-called *spectral methods* that are based on the spectral decomposition of the Laplace-Beltrami operator. In the framework of shape analysis these spectral methods were first proposed in [11]. Based on developments in [16], the *heat kernel signature (HKS)* has been introduced [17]. It assigns each point on an object surface a unique signature based on the fundamental solution of the geometric heat equation. The latter is a partial differential equation (PDE) that contains in its spatial part the Laplace-Beltrami operator and describes the time evolution of heat on an objects' surface. Later, a scale invariant extension of this approach was developed in [5]. In [1] another feature descriptor inspired by the Schrödinger equation was proposed. This feature descriptor is called the *wave kernel signature (WKS)* and represents the average probability of measuring a quantum mechanical particle at a specific location. For both descriptors, the spectral decomposition of the incorporated Laplace-Beltrami operator leads to a series expression of its eigenfunctions and eigenvalues. The contributions in such a series are ordered in the sense that especially the first terms contain the low frequency components describing the macroscopic (global) properties of a shape. Thus, taking into account a corresponding part of the spectral components yields a feature descriptor robust to local errors such as (high frequent) noise but vulnerable to global distortions such as e.g. changes in shape topology.

Our Contributions. In this paper we report on our ongoing investigation of the number of eigenfunctions employed for constructing the HKS and WKS, evaluated with respect to the shape correspondence task. We are not aware of a thorough study of this aspect in the previous literature. In many publications the number of eigenfunctions is set to a fixed value (e.g. first 300 eigenfunctions) without further explanations, representing a very defensive, heuristic choice by our computational experience. With our paper we make an attempt to fill this gap in the current literature. Furthermore, we especially evaluate the HKS and WKS using a much smaller amount of eigenfunctions than usually employed, leading to some interesting conclusions and potential new challenges.

II. THEORETICAL BACKGROUND

In this section we introduce the basic facts that are necessary to define the shape correspondence framework.

A. Almost Isometric Shapes

The bounding surface of a three dimensional geometric object is a two dimensional curved object, embedded into the three dimensional Euclidean space. It is natural to model

Institute of Mathematics, Brandenburg Technical University, Platz der Deutschen Einheit 1, 03046, Cottbus, Germany {dachsel,breuss,hoeltgen}@b-tu.de

shapes as compact two dimensional Riemannian manifolds $\mathscr{M}$, equipped with metric tensor $g \in \mathbb{R}^{2\times 2}$. In this setting, two shapes $\mathscr{M}$ and $\tilde{\mathscr{M}}$ may be considered as *isometric* if there is a mapping T that unfolds one surface onto the other, thereby preserving the intrinsic distances of the unfolded surface. From the mathematical point of view there exists a smooth homeomorphism $T : \mathscr{M} \to \tilde{\mathscr{M}}$ with

$$d_{\mathscr{M}}(x_i,x_j) = d_{\tilde{\mathscr{M}}}(T(x_i),T(x_j)) \quad \forall x_i,x_j \in \mathscr{M}, \tag{1}$$

where $d_{\mathscr{M}}(x_i,x_j)$ is the intrinsic distance taken on manifold $\mathscr{M}$. The intrinsic distance can be thought as the shortest curve along the surface $\mathscr{M}$ connecting x_i and x_j.

As indicated, the notation of isometric shapes appears too restrictive for many applications [4]. Many shapes surrounding us in the world appear with additional small elastic deformations. These occur by either the transformation itself (e.g. as in elastic bending), by geometric noise in datasets, or by transferring a continuously described shape into a numerical framework which may act as a small distortion on the intrinsic distance. We call two shapes $\mathscr{M}$ and $\tilde{\mathscr{M}}$ *almost isometric*, if there exists a transformation $S : \mathscr{M} \to \tilde{\mathscr{M}}$ with

$$d_{\mathscr{M}}(x_i,x_j) \approx d_{\tilde{\mathscr{M}}}(S(x_i),S(x_j)) \quad \forall x_i,x_j \in \mathscr{M}. \tag{2}$$

B. Heat and Schrödinger Equation on Shapes

The common property of the considered PDEs is that the incorporated spatial derivatives have the format of the Laplace-Beltrami operator. Note that the latter is identical to the standard Laplace operator when considering the PDEs in the Euclidean plane, the Laplace-Beltrami operator just takes additionally into account the geometric properties of curvature of a manifold in 3D by making use of tools from differential geometry [7]. Consequently, the Laplace-Beltrami operator is defined on a smooth manifold $\mathscr{M}$.

Turning to the mathematical formulation of the *Laplace-Beltrami operator*, let us recall that for a given parameterisation of a two dimensional manifold, we can express it in local coordinates:

$$\Delta_{\mathscr{M}} u = \frac{1}{\sqrt{|g|}} \sum_{i,j=1}^{2} \partial_i \left(\sqrt{|g|} g^{ij} \partial_j u \right), \tag{3}$$

where $u : \mathscr{M} \to \mathbb{R}$ is a scalar function, g^{ij} are the components of the inverse of the metric tensor and $|g|$ is its determinant.

The *geometric heat equation* describes how heat would propagate along a surface $\mathscr{M}$. The corresponding initial-boundary value problem can be formulated as

$$\begin{cases} \partial_t u(x,t) = \Delta_{\mathscr{M}} u(x,t) & x \in \mathscr{M}, t \in \mathbb{R}^+ \\ u(x,0) = u_0 & \\ \langle \nabla_{\mathscr{M}} u, n \rangle = 0 & x \in \partial\mathscr{M} \end{cases} \tag{4}$$

where u_0 is a given heat distribution. Many shapes appear as closed Riemannian manifold with $\partial\mathscr{M} = \emptyset$, where boundary conditions do not appear. For the case $\mathscr{M}$ has boundaries, we additionally require u to satisfy the homogeneous Neumann boundary conditions, where n is the normal vector to the boundary. In this context the inner product $\langle .,. \rangle$ lives in the tangent space. This choice conserves the amount of heat $\|u\|^2_{L_2(\mathscr{M})} = \text{const}\ \forall t \in \mathbb{R}^+$.

The free, time-dependent *Schrödinger equation*

$$\begin{cases} i\partial_t u(x,t) = \Delta_{\mathscr{M}} u(x,t) & x \in \mathscr{M}, t \in \mathbb{R}_+ \\ u(x,0) = u_0 & \\ \langle \nabla_{\mathscr{M}} u, n \rangle = 0 & x \in \partial\mathscr{M} \end{cases}, \tag{5}$$

where i is the imaginary unit, allows to study how a free and massive quantum particle would move on the surface $\mathscr{M}$. In quantum mechanics, the dynamics of a particle is described by its complex wave function $u(x,t)$ and its probability amplitude, whose square norm $\|u\|^2_{L_2(\mathscr{M})}$ is equal to the probability density for finding the particle at a specific position for a fixed t. In this context u_0 has the interpretation of an initial wave package.

Separation of Variables. First, we assume that the solution will take the form $u(x,t) = \phi(x)T(t)$ due to the fact that we are working with linear and homogeneous partial differential equations. This approach works because if the product of two functions ϕ and T of independent variables x and t is a constant, each function must separately be a constant. At the end, we are able to separate the equations to get a function of only t on one side and a function of only x on the other side

$$\kappa \frac{\partial_t T(t)}{T(t)} = \frac{\Delta_{\mathscr{M}} \phi(x)}{\phi(x)} = \text{const} = -\lambda, \tag{6}$$

where κ summarizes both equations ($\kappa = 1$ for heat equation, $\kappa = i$ for Schrödinger equation), and $-\lambda$ is called the separation constant which is arbitrary for the moment. This leaves us with two new equations, namely an ordinary differential equation for the temporal component

$$\partial_t T(t) = -\kappa\lambda T(t) \quad t \in \mathbb{R}_+ \tag{7}$$

and the spatial part takes the form of the Helmholtz equation

$$\begin{cases} \Delta_{\mathscr{M}} \phi(x) = -\lambda \phi(x) & x \in \mathscr{M} \\ \langle \nabla_{\mathscr{M}} \phi, n \rangle = 0 & x \in \partial\mathscr{M} \end{cases}, \tag{8}$$

where the value of the constant λ has the meaning of the operator's eigenvalue.

The Spatial Part. The Laplace-Beltrami operator is a self-adjoint operator on the space $L_2(\mathscr{M})$ (since we assumed the shapes to be compact). This implies that the *Helmholtz equation*

$$\begin{cases} \Delta_{\mathscr{M}} \phi_k(x) = -\lambda_k \phi_k(x) & x \in \mathscr{M} \\ \langle \nabla_{\mathscr{M}} \phi_k, n \rangle = 0 & x \in \partial\mathscr{M} \end{cases} \quad k \in \{1, \ldots \infty\} \tag{9}$$

has infinite non-trivial solutions for certain (discrete) values called eigenvalues, and corresponding eigenfunctions, which is a result of the spectral theorem. The ordered spectrum of eigenvalues $0 = \lambda_1 < \lambda_2 \leq \ldots \leq \lambda_\infty$ and corresponding eigenfunctions $\phi_1, \phi_2, \ldots, \phi_\infty$ form an orthonormal basis of $L_2(\mathscr{M})$, and constant functions are solutions of the Helmholtz equation with eigenvalue 1 (only for Neumann boundary conditions or no shape boundaries).

It is well known that the eigenfunctions are a natural generalization of the classical Fourier basis to functions on shapes. Let us note that the physical interpretation of the Helmholtz equation is the following. The shape of a 3D object can be thought of as a vibrating membrane, the ϕ_k can be interpreted as its vibration modes whereas the λ_k have the meaning of the corresponding vibration frequencies, sorted from low to high frequencies, as shown in Figure 4

The Temporal Part. For each $k \in \{0, \dots \infty\}$ there is an ordinary differential equation (7) left, corresponding to $\lambda \equiv \lambda_k$, which can be solved by integrating both sides using the indefinite integral. This leads to

$$\int \frac{1}{T(t)} \mathrm{d}T(t) = -\kappa\lambda_k \int \mathrm{d}t \quad \Rightarrow \quad T(t) = \alpha_k e^{-\kappa\lambda_k t}, \quad (10)$$

where the integration constant α_k should satisfy the initial condition of the k^{th} eigenfunction. The final product solution then reads as

$$u_k(x,t) = \alpha_k e^{-\kappa\lambda_k t} \phi_k(x). \quad (11)$$

The principle of superposition says that if we have several solutions to a linear homogeneous differential equation then their sum is also a solution. Therefore, a closed-form solution of the heat equation in terms of a series experession can be written as

$$u(x,t) = \sum_{k=1}^{\infty} \alpha_k e^{-\lambda_k t} \phi_k(x), \quad (12)$$

and the solution of the Schrödinger equation reads as

$$u(x,t) = \sum_{k=1}^{\infty} \alpha_k e^{-i\lambda_k t} \phi_k(x), \quad (13)$$

where the coefficient α_k fulfill the initial condition.

Heat Kernel Signature. The coefficients α_k in our expansion can be computed by using the L^2 inner product

$$\alpha_k = \langle u_0, \phi_k \rangle_{L^2(\mathscr{M})} = \int_{\mathscr{M}} u_0(y)\phi_k(y)\,\mathrm{d}y \quad (14)$$

such that we have

$$u(x,t) = \sum_{k=1}^{\infty} \left(\int_{\mathscr{M}} u_0(y)\phi_k(y)\,\mathrm{d}y \right) e^{-\lambda_k t}\phi_k(x) \quad (15)$$

$$= \int_{\mathscr{M}} u_0(y) \left(\sum_{k=1}^{\infty} e^{-\lambda_k t}\phi_k(y)\phi_k(x) \right) \mathrm{d}y. \quad (16)$$

The term inside the brackets is called the *heat kernel* $K(x,y,t)$, and it describes the amount of heat transmitted from x to y after time t. By setting the initial condition to be a delta heat distribution at the position y with $u_0(y) = \delta_x(y)$, we thus obtain after [17] the *heat kernel signature*

$$\mathrm{HKS}(x,t) = \sum_{k=1}^{\infty} e^{-\lambda_k t} \left|\phi_k(x)\right|^2, \quad (17)$$

where the shifting property of the delta distribution $f(x) = \int_{\mathscr{M}} f(y)\delta_x(y)\,\mathrm{d}y$ was used. The quantity $\mathrm{HKS}(x,t)$ describes the amount of heat present at point x at time t.

Wave Kernel Signature. The *wave kernel signature* [1] is defined to be the time-averaged probability of detecting a particle of a certain energy distribution at the point x, formulated as

$$\mathrm{WKS}(x,t) = \lim_{T\to\infty} \frac{1}{T} \int_0^T |u|^2 \mathrm{d}t = \sum_{k=1}^{\infty} |\alpha_k|^2 \left|\phi_k(x)\right|^2. \quad (18)$$

Furthermore, $\alpha_k = \alpha(e_k)$ becomes a function of the energy distribution e_k of the quantum mechanical particle and can be chosen as a log-normal distribution i.e.

$$|\alpha_k|^2 = \exp\left(\frac{-(e - \log\lambda_k)^2}{2\sigma^2} \right), \quad (19)$$

where the variance of the energy distribution is denoted by σ, see again [1] for more details.

C. Discretization Aspects

While we have described now the analytical setting, we have to translate the analytical set-up into a discrete format allowing to deal with shape data.

Discrete Surfaces. A suitable surface representation is given by a triangular mesh. In more detail, a triangulated surface is given by the tuple $\mathscr{M}_d = (P,T)$. The point cloud $P := \{x_1, \dots, x_N\}$ contains the finite number of vertices (given as coordinate points in $\mathbb{R}^3$) a shape consists of. The entire mesh can be formed by connecting the vertices x_i so that one obtains two-dimensional linear triangles. Therefore, the set of linear triangles T contains the neighborhood relations between vertices forming a triangle. Further, we sub-divide the meshed surface as follows:

$$\mathscr{M}_d = \bigcup_{i=1}^{N} \Omega_i \quad \text{and} \quad \Omega = \mathrm{diag}\,(\Omega_1, \dots, \Omega_N) \in \mathbb{R}^{N\times N} \quad (20)$$

where Ω_i is the barycentric cell volume, surrounding the vertex x_i, as shown in Figure 1.

Discrete Laplace-Beltrami Operator. Many schemes have been proposed to estimate the Laplace-Beltrami operator for a triangular meshed surface [2], [14], [15]. A commonly used method is the cotangent weight scheme introduced in [13]. As a result, for a function defined on a triangular mesh the discrete Laplace-Beltrami operator $L \in \mathbb{R}^{N\times N}$ reduces to the following simple sparse matrix representation

$$L_{ij} = \begin{cases} -\sum\limits_{j\in N_i} w_{ij} & \text{if } x_i = x_j \\ w_{ij} & \text{if } x_i \neq x_j \text{ and } x_j \in N_i, \\ 0 & \text{else} \end{cases} \quad (21)$$

where N_i denotes the set of points adjacent to x_i. As shown in Figure 1, the weights w_{ij} of the edge (x_i, x_j) can be classified into interior E_i and boundary edges E_b, respectively,

$$w_{ij} = \begin{cases} \frac{\cot\alpha_{ij} + \cot\beta_{ij}}{2} & \text{if } (x_i,x_j) \in E_i \\ \frac{\cot\alpha_{ij}}{2} & \text{if } (x_i,x_j) \in E_b \end{cases}. \quad (22)$$

as also shown in Figure 1. Furthermore, α_{ij} and β_{ij} denote the two angles opposite to the edge (x_i, x_j), for details we

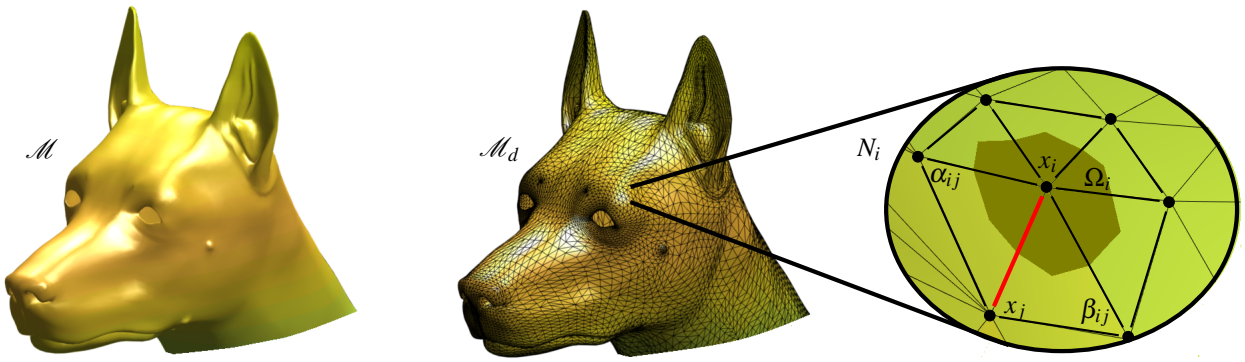

Fig. 1. Continuous and discrete representation of a shape. **Left:** In the continuous setting a shape is modeled by a two dimensional Riemannian manifold $\mathcal{M}$. **Middle:** Its discrete approximation $\mathcal{M}_d$ is given by a point cloud P, where the points are connected by non-uniform and linear triangles T. **Right:** For the construction of the discrete Laplace-Beltrami operator at the point x_i, it requires the set of adjacent points N_i, the surrounding cell volume Ω_i and the two angles α_{ij} and β_{ij} opposite to the edge (x_i, x_j).

refer to the mentioned source. The eigenfunctions and eigenvalues of the discrete Laplacian are computed by performing the generalized eigen-decomposition

$$L\phi_k = -\lambda_k \Omega \phi_k\,, \quad k \in \{1,\ldots,N\}\,, \tag{23}$$

However, an important practical aspect of the eigen-decomposition is that computing a full spectrum is very time and memory consuming (e.g. all eigenfunctions have to be stored in a dense $\mathbb{R}^{N\times N}$ matrix). Therefore, only the first $\tilde{N} \ll N$ of the eigenvalues in increasing order and corresponding eigenfunctions are computed. The eigenvalue $\lambda_1 = 0$ belongs to the constant eigenfunction ϕ_1, containing no information useful for shape correspondence.

The discrete HKS and WKS read for a given point x_i finally

$$\mathrm{HKS}(x_i,t) = \sum_{k=2}^{\tilde{N}} e^{-\lambda_k t} \left|\phi_k(x_i)\right|^2 \quad \text{and} \tag{24}$$

$$\mathrm{WKS}(x_i,t) = \sum_{k=2}^{\tilde{N}} \left|\alpha_k\right|^2 \left|\phi_k(x_i)\right|^2 . \tag{25}$$

Discrete Time and Energy Scale. For the HKS, the time axis is sampled at 100 samples, $t_1,\ldots,t_{100}$, where the time is logarithmically scaled over the time interval with $t_1 = 4\ln 10/\lambda_{\tilde{N}}$ and $t_{100} = 4\ln 10/\lambda_2$. The energy scale of the WKS becomes $e_1 = \log(\lambda_2) + 2\sigma$ and $e_{100} = \log(\lambda_{\tilde{N}}) - 2\sigma$, and the parameters were set as described in [1].

III. THE CORRESPONDENCE PROBLEM

For two points $x_i \in \mathcal{M}_d$ and $\tilde{x}_i \in \tilde{\mathcal{M}}_d$ the condition for a point-wise correspondence can be written as a minimisation problem:

$$(x_i,\tilde{x}_j) \;\Leftrightarrow f(\tilde{x}_j) = \min_{k=1,\ldots,\tilde{N}} \{d_{FD}(x_i,\tilde{x}_k)\}\,. \tag{26}$$

where $d_{\mathrm{FD}}(x_i,\tilde{x}_j)$ is the *feature distance*.

For the HKS the squared distance is measured by computing a normalised L_2-norm

$$d_{\mathrm{HKS}}(x_i,\tilde{x}_j) = \left\{ \int_{t_1}^{t_{100}} \left(\frac{|\mathrm{HKS}(x_i,t) - \mathrm{HKS}(\tilde{x}_j,t)|}{\int_{\mathcal{M}} \mathrm{HKS}(x,t)\mathrm{d}x} \right)^2 \mathrm{d}\log t \right\}^{\frac{1}{2}} \tag{27}$$

and the WKS uses a distance based on the L_1-norm of the normalised signature difference

$$d_{\mathrm{WKS}}(x_i,\tilde{x}_j) = \int_{e_1}^{e_{100}} \left| \frac{\mathrm{WKS}(x_i,e) - \mathrm{WKS}(\tilde{x}_j,e)}{\mathrm{WKS}(x_i,e) + \mathrm{WKS}(\tilde{x}_j,e)} \right| \mathrm{d}e. \tag{28}$$

IV. EXPERIMENTAL RESULTS

A. Evaluation Measure and Dataset

In general, we perform a dense point-to-point correspondence, involving all vertices the shapes are made off. We investigate the quality of the established correspondences at hand of several quality measures that are standard in the abovementioned literature.

The tests we discuss here are chosen so that they are in some sense generic, as they are not tuned to a specific class of shapes with some special property. Our aim is to study a typical setting for the shape correspondence problem in detail and to get an insight into typical phenomena occuring when approaching the task. The dog shapes appear to be suitable for this proceeding, as they show a reasonable range of mesh widths and transformations, but not topological changes (representing in shape matching a hard problem to resolve by itself which is beyond the scope of this paper) that may especially hinder to find correspondences by the first few eigenfunctions.

We concentrate in this paper on discussing our current findings in analyzing mutual influences of eigenfunctions, eigenvalues (i.e. ordering of eigenfunctions), and matching accuracy of spectral methods for shape correspondence. In detail, the experiments are evaluated as follows.

Hit Rate. The percentual *hit rate* is defined as $TP/(TP+FP)$, where TP and FP are the number of true positives and false positives, respectively.

Fig. 2. The dog class of the TOSCA data set. The transformed shapes are almost isometric modifications of the reference shape (left).

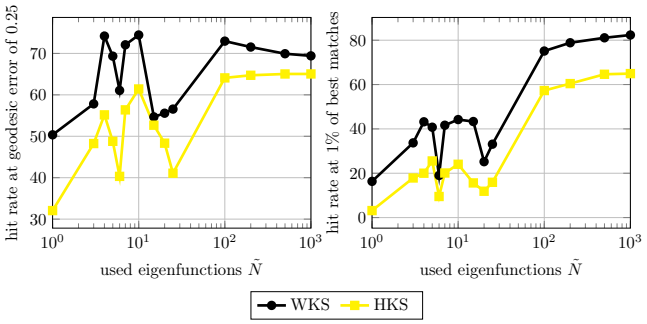

Fig. 3. Here we compared both the HKS and the WKS for finding correspondences within a geodesic error of 0.25 (left) and correct correspondences at 1% of best matches (right) as a function of the used eigenfunctions. For large $\tilde{N}$, the performance goes into saturation. Small $\tilde{N}$ leads roughly to a similar quality in terms of an acceptable geodesic errors but unstable performance.

Cumulative Match Characteristic (CMC). The CMC curve evaluates the hit rate for finding true corresponding pairs within the first 1% of best matches. Thereby the best matches are those with the smallest feature distance, arranged in increasing order.

The Geodesic Error. For the evaluation of the correspondence quality, we followed the Princeton benchmark protocol [9]. This procedure evaluates the precision of the computed matching x_i by determining how far are those away from the actual ground-truth correspondence x^*. Therefore a normalised intrinsic distance $d_{\mathscr{M}}(x_i,x^*)/\sqrt{A_{\mathscr{M}}}$ on the transformed shape is introduced. Finally, we accept a matching to be true if the normalised intrinsic distances are smaller than the threshold 0.25.

Dataset. For the experiment nine dog shapes are used, taken from the TOSCA data set [4], available in the public domain as shown in Figure 2.

B. Influence of the Amount of Eigenfunctions to Shape Correspondence

For the first experiment we increase the number of used ordered eigenfunctions, starting from $\tilde{N} = 3$ and end up to $\tilde{N} = 1000$, and study the quality of finding correspondences. Note that we average in this experiment over all correspondence computations performed over the given data set, see Figure 2.

The evaluation in Figure 3 shows how the matching precision of the HKS and WKS depends on the number of used eigenfunctions. After taking into account about hundred eigenfunctions the performance for both descriptors goes into saturation, i.e. it does not increase significantly anymore. Considering especially the comparison of correct correspondences within the geodesic threshold, displayed in Figure 3 (left), it is remarkable that the results for a very small spectrum $\tilde{N} \approx 10$ are similar to the ones for the large spectrum $\tilde{N} \approx 1000$. Especially the WKS descriptor gains already reasonable results in the regime of the small spectrum.

We also see, however, that within the small spectrum the correspondence quality suffers by large variations including a performance collapse of $15\% - 20\%$ at a specific range of eigenfunctions, $\tilde{N} \approx 3$ and $\tilde{N} \approx 20$ for both descriptors. On the other hand, the performance is stabilized and stays stable for a larger amount of eigenfunctions.

It would surely be interesting to attempt to tune the small spectrum in such a way that it becomes more stable, e.g. by removing eigenfunctions that result in a performance loss. In this paper, such considerations motivate us to explore the phenomena potentially encountered when using a small spectrum.

C. Shape Correspondence Using a Small Spectrum

The test just discussed above shows that it may be worth the effort to inspect in more detail the situation of the small spectrum of eigenfunctions. To this end we will also employ a finer sampling of the error behaviour for the small range of eigenfunctions as in the first test.

First of all we study the eigenfunctions itself for the reference dog shape and three arbitrarily selected almost isometric counterparts from our test data set. We pay attention to the small spectrum where $\tilde{N}$ is ranging from 3 to 25. By comparing the eigenfunctions on the reference shape and transformed shape, they should be similar since eigenfunctions belonging to low frequencies are stable under almost isometric transformations. However, as visualized in Figure 4 for selected examples of eigenfunctions, not all appear to be similar. In order to make this impression quantitative, we define an averaged error with respect to the reference shape (dog0),

$$e(\phi_i, \tilde{\phi}_i) = \frac{1}{N} \sum_{k=1}^{N} \left| |\phi_i(x_k)| - |\tilde{\phi}_i(x_k)| \right| , \qquad (29)$$

where ϕ_i and $\tilde{\phi}_i$ are the i^{th} eigenfunctions on the reference and transformed shape, respectively. Then, we compare the matching performance of the HKS and WKS for the selected shapes as a function of eigenfunctions, considered at the small spectrum, as shown in Figure 5.

The results show that there is a surprisingly large error when comparing the first few eigenfunctions of the Laplace-Beltrami operator, as seen in Figure 5. For interpretation one may consider the analogy to approximate a given signal by the first few terms of a Fourier series; it seems that the dog shape incorporates in the low frequency range a few frequencies that are not highly significant and therefore not captured equally well by shape variations. We conjecture that

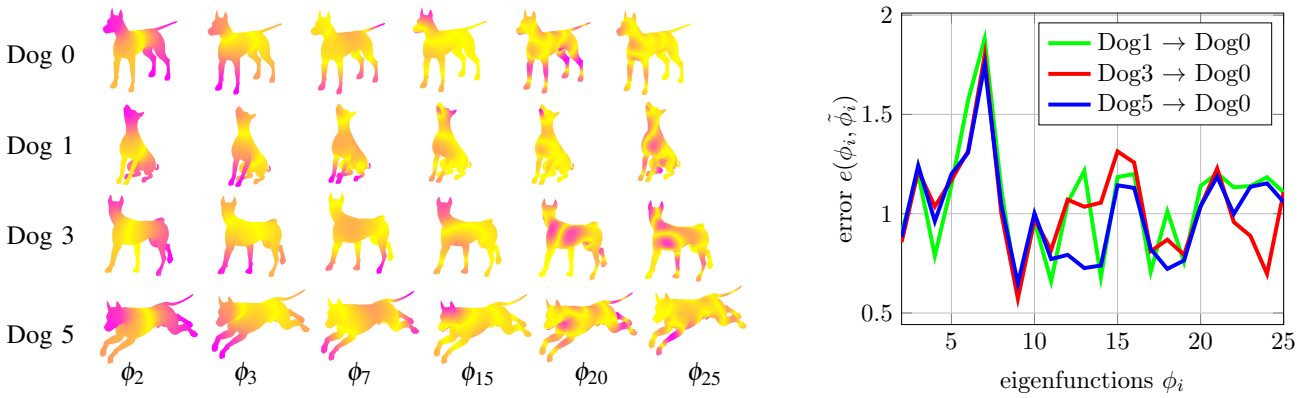

Fig. 4. Comparing selected eigenfunctions on the dog and their error under almost isometric transformations. **Left:** The absolute value of the eigenfunction of the Laplace-Beltrami operator computed on examples of the dog dataset. The colors represent the values of the eigenfunctions, pink being the most positive and yellow are almost zero values. **Right:** Error of the eigenfunctions of the reference shape (dog 0) and the almost isometric counterparts (dog 1, dog 3, dog 5). The smaller the error, the more stable are the eigenfunctions under almost isometric transformations.

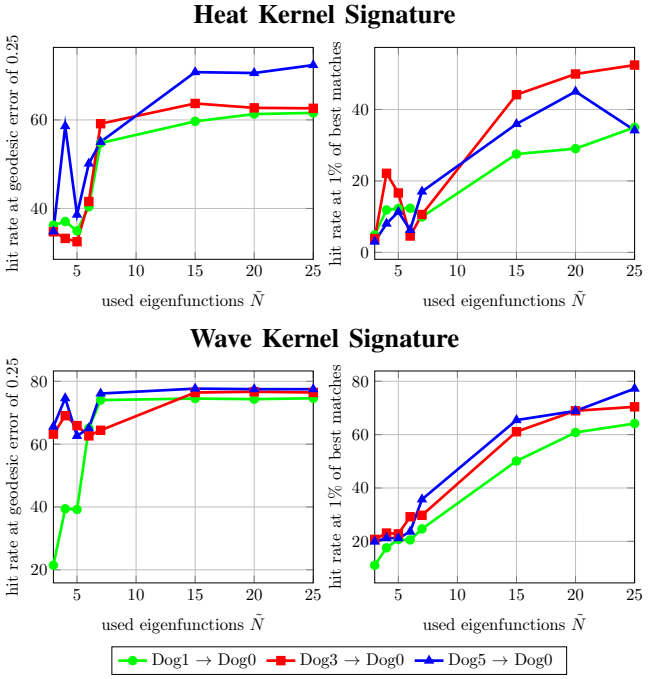

Fig. 5. The evaluation of shape correspondence for the selected dog shapes using the HKS and WKS. The performance is plotted as a function of the used small spectrum.

this is a phenomenon that can be found in a similar way for some low frequencies in other shapes. The phenomenon gets stabilized after taking into account a few more eigenfunctions here. Let us stress that this interesting aspect is not visible in tests as performed usually in the literature where error averages over large data sets with many different shapes are computed.

Secondly, we also observe a correlation between the error in matching eigenfunctions of the Laplace-Beltrami operator and the shape matching performance with HKS and WKS when comparing Figure 5 to results given in Figure 3. After the discussion above, it is evident that this is mainly observable in the first few eigenfunctions, yet the WKS may still achieve in some cases high accuracy in terms of admissible geodesic error. One may also infer that the WKS is often more robust against differences in eigenfunctions at low frequencies than the HKS. This appears to be physically intuitive since solutions of the Schrödinger equation bear a more complex wave interaction pattern (arguably the main point leading to high accuracy) than the smoothly varying solutions of the heat equation (where consequently the low frequencies carry most information).

One may also conjecture that the occurence of a very low error as for $i = 9$ seems to have a significant stabilizing effect, especially concerning best matches. This effect may also be present in the Dog3→Dog0 experiment in the range of 20 to 25 eigenfunctions. Comparing the red lines in Figure 5 and HKS best matches in Figure 3 (top right), we see that the hit rates in the other two experiments deteriorate as they do not benefit from the conjectured mechanism.

V. CONCLUSION AND FURTHER WORK

The computation of shape correspondences is a computationally intensive task. Therefore it would be highly desirable to develop a spectral method relying only on the first few terms of the corresponding series expansion. We have pointed out some aspects of approximations using such small spectra at hand of a typical shape correspondence experiment. We think that our discussion illuminates some points that can be important for the construction of such a method.

In the future we plan to pursue this open issue. For this it will be imperative in a first step to perform more experiments with other shapes, and to validate the aspects we found in this paper also at hand of simple, specifically constructed shapes.

REFERENCES

[1] M. Aubry, U. Schlickewei, and D. Cremers, "The wave kernel signature: a quantum mechanical approach to shape analysis," *IEEE Computer Vision Workshops (ICCV Workshops)*, pp. 1626–1633, 2011.
[2] M. Belkin, J. Sun, and Y. Wang, "Discrete Laplace operator on meshed surfaces," in *Proceedings of SOCG*, 2008, pp. 278–287.
[3] P. J. Besl and N. D. McKay, "A method for registration of 3-d shapes," in *IEEE Trans. Pattern Anal. Mach. Intell. 14*, 1992, pp. 239–256.

[4] A. M. Bronstein, M. M. Bronstein, and R. Kimmel, *Numerical geometry of non-rigid shapes*. Springer, 2009.
[5] M. M. Bronstein and I. Kokkinos, "Scale-invariant heat kernel signatures for non-rigid shape recognition," in *Proc. International Conference on Computer Vision and Pattern Recognition*, 2010, pp. 1704–1711.
[6] Y. Chen and G. Medioni, "Object modelling by registration of multiple range images," in *Image Vision Comput. 10*, 1992, pp. 145–155.
[7] M. P. Do Carmo, *Differential geometry of curves and surfaces: revised and updated second edition*. Dover Puplications, 2016.
[8] M. Kilian, N. J. Mitra, and H. Pottmann, "Geometric modeling in shape space," in *In Proceedings of SIGGRAPH*, vol. 26, no. 3, 2007.
[9] V. G. Kim, Y. Lipman, and T. A. Funkhouser, "Blended intrinsic maps," in *ACM Transactionson Graphics*, vol. 30, no. 4, 2011.
[10] M. Levoy, K. Pulli, B. Curless, S. Rusinkiewicz, D. Koller, L. Pereira, M. Ginzton, S. Anderson, J. Davis, J. Ginsberg, and J. F. D. Shade, "The digital michelangelo project: 3d scanning of large statues." in *In Proceedings of SIGGRAPH*, 2000, pp. 131–144.
[11] B. Lévy, "Laplace-Beltrami eigenfunctions towards an algorithm that 'understands' geometry." in *Int. Conf. on Shape Modeling and Applications*, 2006.
[12] J. Maintz and V. M., "A survey of medical image registration," in *Medical Image Analysis 2*, 1998, pp. 1–36.
[13] M. Meyer, M. Desbrun, P. Schröder, and A. H. Barr, "Discrete differential-geometry operators for triangulated 2-manifolds," in *In Visualization and Mathematics III*. Springer, 2002, pp. 35–57.
[14] U. Pinkall and K. Polthier, "Computing discrete minimal surfaces and their conjugates," *Experimental Mathematics*, vol. 2, no. 1, pp. 15–36, 1993.
[15] M. Reuter, F. E. Wolter, and N. Peinecke, "Laplace-Beltrami spectra as shape-DNA of surfaces and solids," *Computer-Aided Design*, vol. 38, no. 4, pp. 342–366, 2006.
[16] R. Rustamov, "Laplace-Beltrami eigenfunctions for deformation invariant shape representation," in *Symp. Geometry Processing*, 2007, pp. 225–233.
[17] J. Sun, M. Ovsjanikov, and L. Guibas, "A concise and provably informative multi-scale signature based on heat diffusion," *Computer Graphics Forum*, vol. 28, no. 5, pp. 1383–1392, 2009.